

Supporting information for

**Friction and conductance imaging of  $sp^2$ - and  $sp^3$ -hybridized  
subdomains on single-layer graphene oxide**

*Hyunsoo Lee<sup>a,b+</sup>, Narae Son<sup>c+</sup>, Hu Young Jeong<sup>d</sup>, Tae Gun Kim<sup>e</sup>, Gyeong Sook Bang<sup>c</sup>, Jong Yun Kim<sup>c</sup>, Gi Woong Shim<sup>c</sup>, Kalyan C. Goddeti<sup>a,b</sup>, Jong Hun Kim<sup>a,b</sup>, Nam Dong Kim<sup>f</sup>, Hyun-Joon Shin<sup>f</sup>, Wondong Kim<sup>g</sup>, Sehun Kim<sup>h</sup>, Sung-Yool Choi<sup>\*c</sup>, and Jeong Young Park<sup>\*a,b</sup>*

<sup>a</sup>Center for Nanomaterials and Chemical Reactions, Institute for Basic Science (IBS),  
Daejeon 305-701, Korea

<sup>b</sup>Graduate School of EEWS, Korea Advanced Institute of Science and Technology (KAIST),  
Daejeon 305-701, Korea

<sup>c</sup>Department of Electrical Engineering and Graphene Research Center, KAIST, 291 Daehak-  
ro, Daejeon, Korea

<sup>d</sup>UNIST Central Research Facilities (UCRF), UNIST, 100 Banyeon-ri, Eonyang-eup, Ulsan,  
Korea

<sup>e</sup>Korea University of Science and Technology (UST), 206 Gajeong-ro, Daejeon 305-350,  
Korea

<sup>f</sup>Pohang Accelerator Laboratory, Pohang 790-834, Korea

<sup>g</sup>Center for Nanometrology, Korea Research Institute of Standards and Science (KRISS), 267  
Gajeong-ro, Yuseong-gu, Daejeon 305-340, Korea

<sup>h</sup>Department of Chemistry and Molecular-Level Interface Research Center, KAIST, 291  
Daehak-ro, Daejeon, Korea

\*To whom correspondence should be addressed. E-mail: jeongypark@kaist.ac.kr

## 1. UV–Vis spectra

Fig. S1 shows a UV–Vis spectrum of GO dissolved in water, exhibiting two absorption peaks in the visible and near-infrared range. The maximum absorption at 229 nm corresponds to  $\pi \rightarrow \pi^*$  transitions of aromatic C–C bonds, and the shoulder at 300 nm originates from  $n \rightarrow \pi^*$  transitions of C–O bonds.<sup>1</sup>

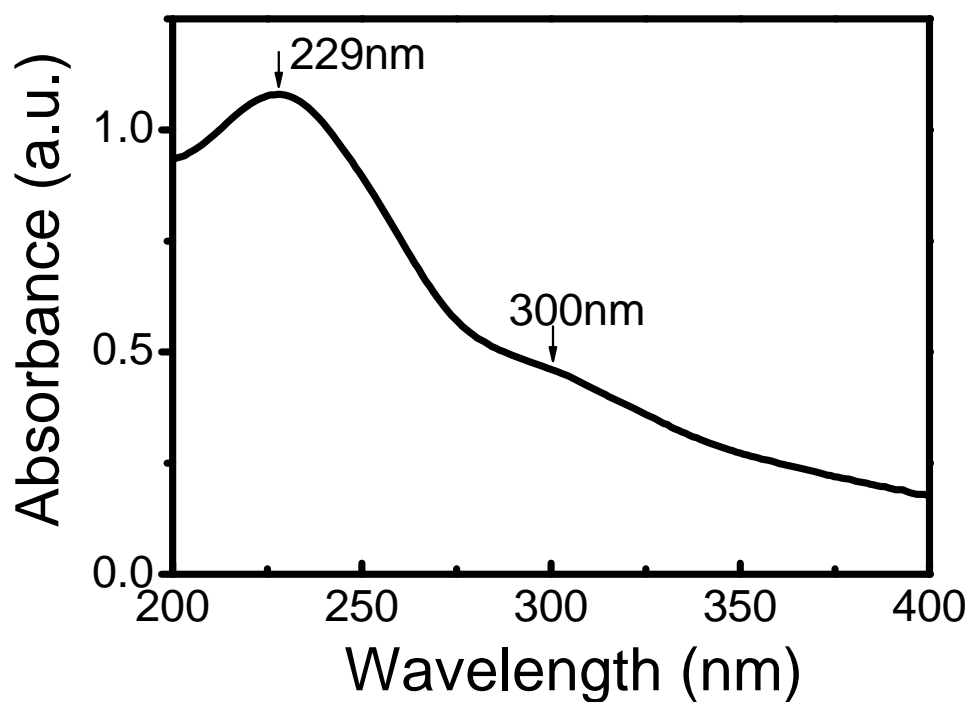


Fig. S1. UV–Vis absorbance spectrum of the GO solution in water.

## 2. Raman spectra

To characterize the structural information for GO (e.g., crystal size and disorder level), micro-Raman spectra (Fig. S2) were obtained using a 514.5 nm laser. The spectra exhibited three main characteristic peaks: G band ( $\sim 1603\text{ cm}^{-1}$ ), D band ( $\sim 1347\text{ cm}^{-1}$ ), and 2D band ( $\sim 2700\text{ cm}^{-1}$ ). The relative intensity ratio of the D and G peaks ( $I_D/I_G$ ) was about 0.975. The feature at  $\sim 2920\text{ cm}^{-1}$  is associated with a D + G combination mode induced by disorder.

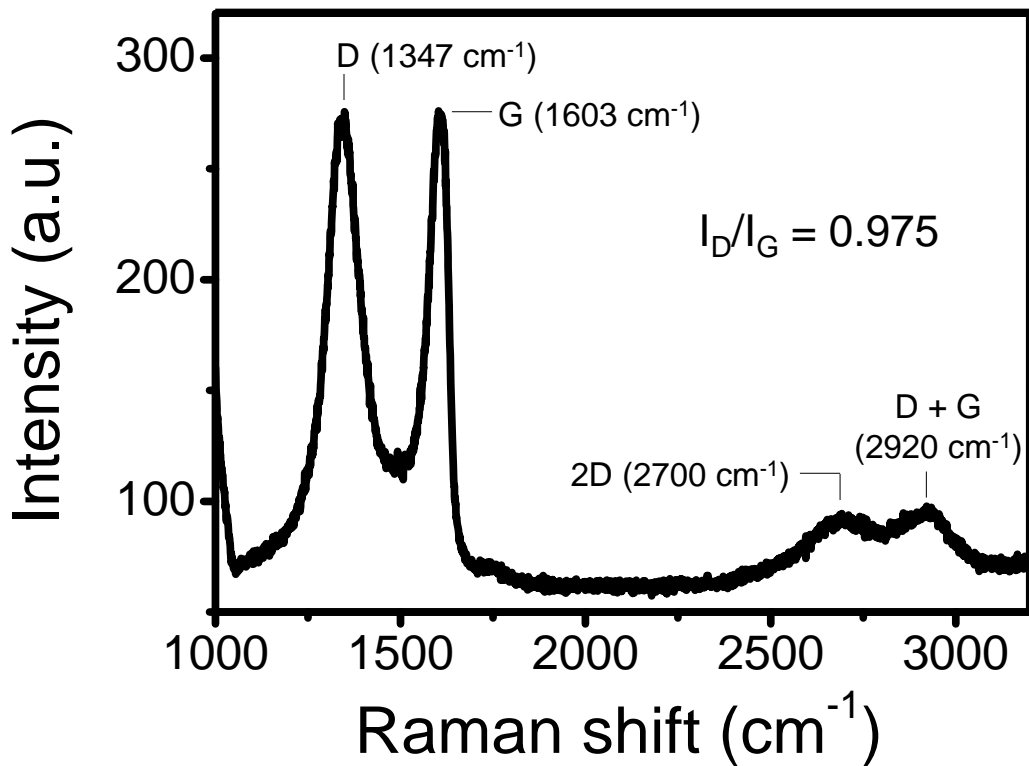


Fig. S2. Raman spectrum of single-layer GO recorded using a 514.5 nm laser and calibrated using the  $521\text{ cm}^{-1}$  Si peak as reference.

### 3. Fourier transform infrared spectra (FT-IR)

FT-IR was used to verify the presence of functional groups in GO. We observed dominant peaks at 3423, 1733, 1619, 1360, 1222 and 1051  $\text{cm}^{-1}$ . The peak at 1619  $\text{cm}^{-1}$  corresponds to C–C bonds associated with skeletal vibrations of the graphitic  $\text{sp}^2$  domains. The other peaks are all attributed to oxygen functional groups: The peak at 3423  $\text{cm}^{-1}$  corresponds to stretching vibrations from O–H bonds of hydroxyl groups or adsorbed water. The peak at 1733  $\text{cm}^{-1}$  is attributed to C=O bonds in carboxylic acid and carbonyl groups. The peaks at 1360, 1222, and 1051  $\text{cm}^{-1}$  correspond to C–O bonds in carboxylic acid, epoxide, and alkoxy groups, respectively.

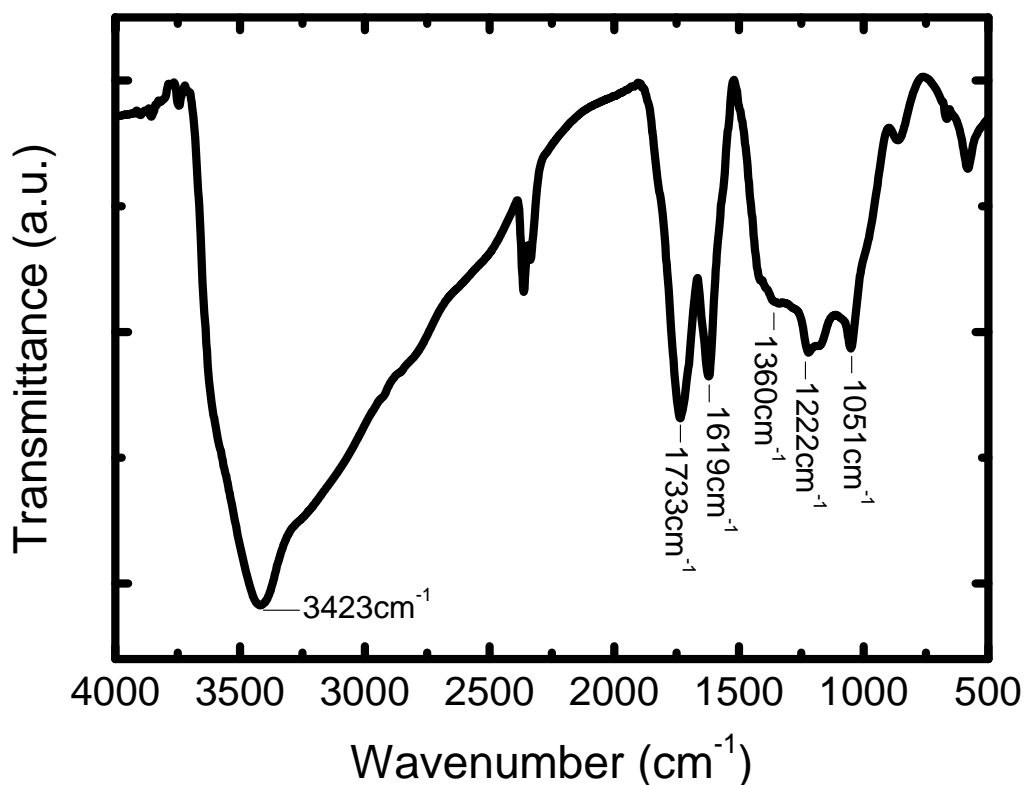


Fig. S3. FT-IR spectrum of GO.

#### 4. X-ray photoelectron spectroscopy (XPS)

XPS was employed to analyze the components of the oxygen functional groups of GO. Fig. S4a shows a wide-scan spectrum characterized by two main peaks: O1s and C1s. The intensity ratio of O/C was about 1.84. The C1s core-level spectrum revealed three major peaks, which are assigned to  $sp^2$  and  $sp^3$  C–C bonds at 284.8 eV; C–O bonds of epoxy groups at 286.9 eV; and carboxylic groups at 288.7 eV in Fig. S4b.<sup>2-5</sup>

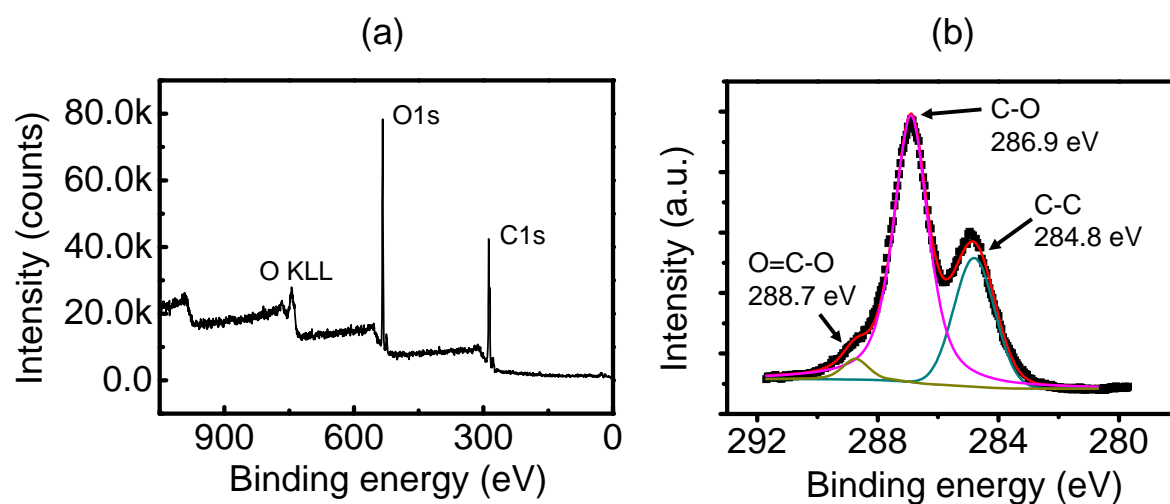


Fig. S4. XPS spectra of GO: (a) wide-scan spectrum and (b) C1s spectrum.

## 5. Height profile of GO on SiO<sub>2</sub>/Si

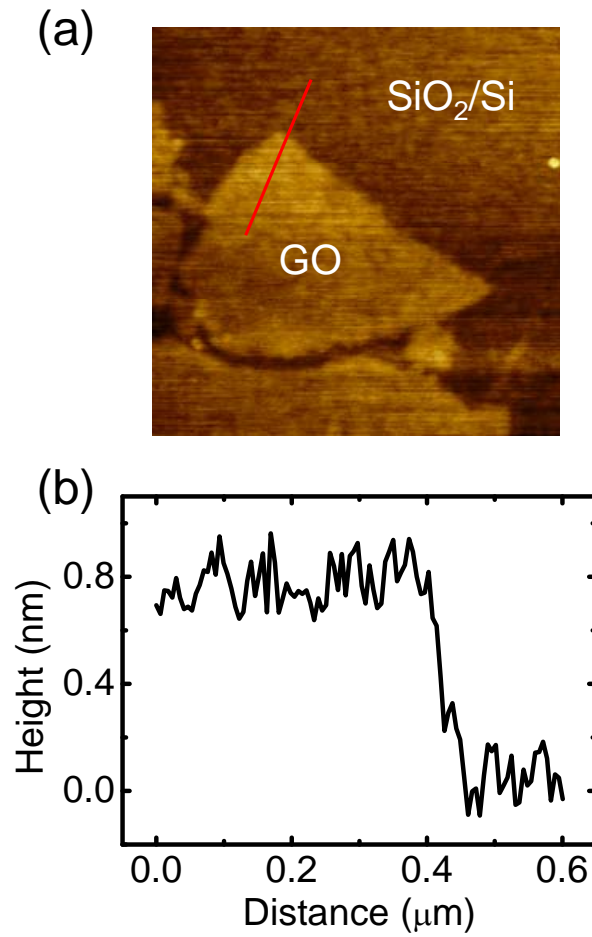


Fig. S5. (a) Topography and (b) cross-section profile (along the red solid line in (a)) of the GO sheet on SiO<sub>2</sub>/*n*-Si. The average height of the GO sheet is about 0.8 nm.

## 6. Friction loop of the GO sheet on SiO<sub>2</sub>/Si

Fig. S6 shows the friction loop for the data in Fig. 3. The regions with sp<sup>2</sup>- and sp<sup>3</sup>-rich phases, and SiO<sub>2</sub> substrate are clearly distinguished. The sp<sup>2</sup>-rich phase does not exactly correspond with the pristine graphene. The GO sheet can have higher friction than that of the SiO<sub>2</sub> substrate due to a high concentration of –OH groups, creating a reactive, polar surface with a higher density of silanol groups on the GO sheet.<sup>6,7</sup>

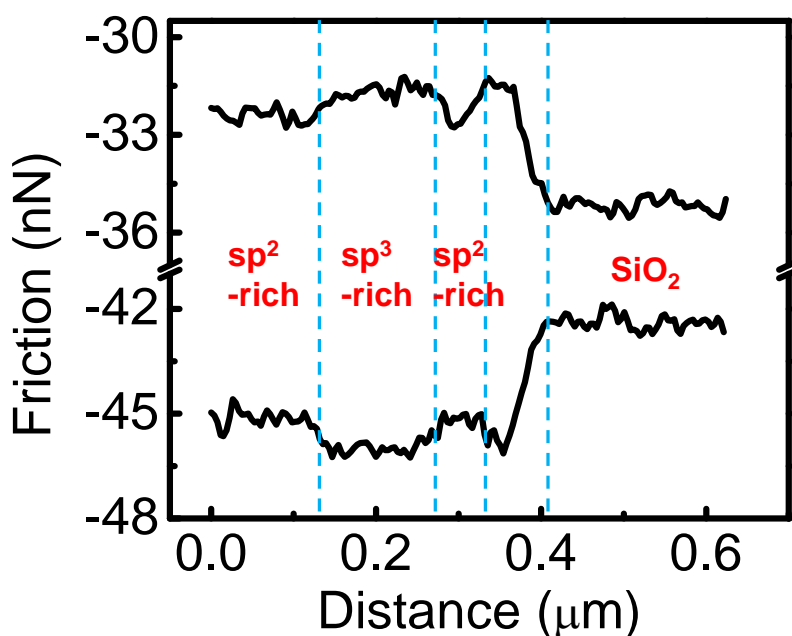


Fig. S6. Friction loop of the GO sheet on SiO<sub>2</sub>/Si substrate.

## 7. Magnified friction image of GO

Fig. S7 shows a friction image with small scans on a mixture of hydroxyl and carboxyl groups, and epoxy bridges within the 2-dimensional carbon layer, which includes both sp<sup>2</sup>- and sp<sup>3</sup>-rich domains. The contrast of friction is clearly shown in Fig. S9b.

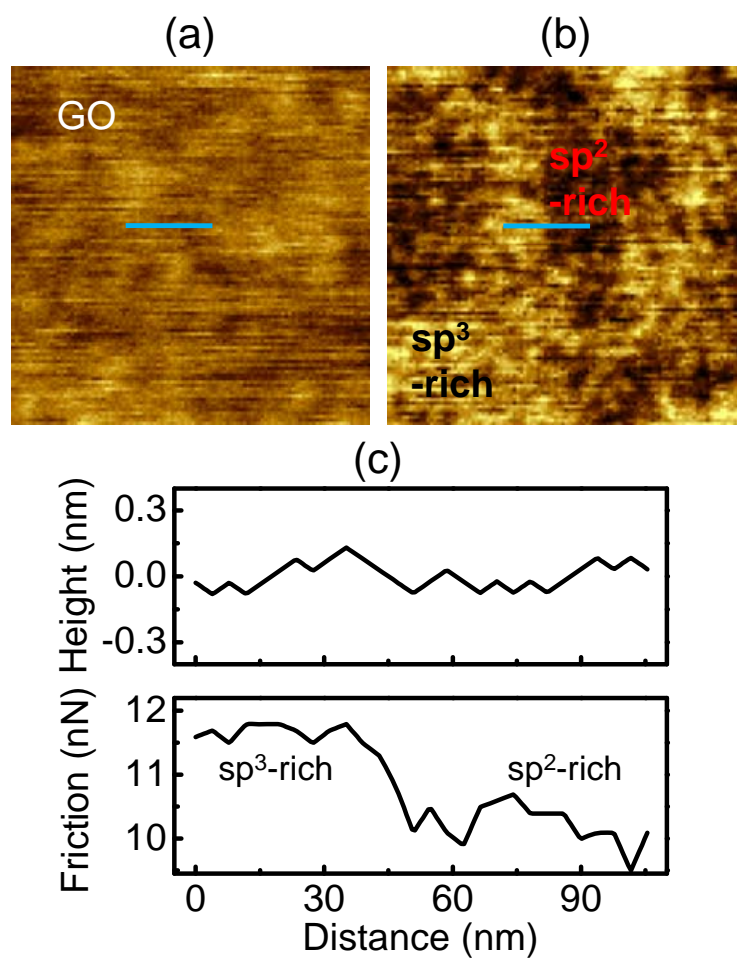


Fig. S7. (a) Topography ( $400 \times 400 \text{ nm}^2$ ) and (b) friction mapping of the GO surface taken using C-AFM. (c) Line profiles of the height and friction along the blue lines in (a) and (b).

## 8. Statistical difference of friction

Fig. S8 shows a histogram showing the statistical difference for friction from multiple GO flakes. It clearly shows two main peaks for the friction on  $\text{sp}^2$ - and  $\text{sp}^3$ -rich regions.

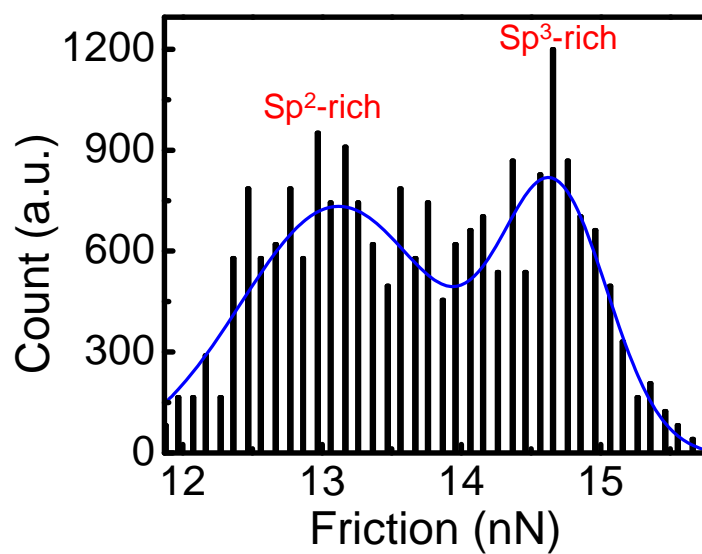


Fig. S8. Histogram of the friction on GO flakes with a Gaussian-fitted blue line.

## 9. Energy levels of a sample junction

Fig. S9 show the energy levels of a sample junction that includes Pt from the C-AFM tip, single-layer GO, SiO<sub>2</sub>, and *n*-Si (100).

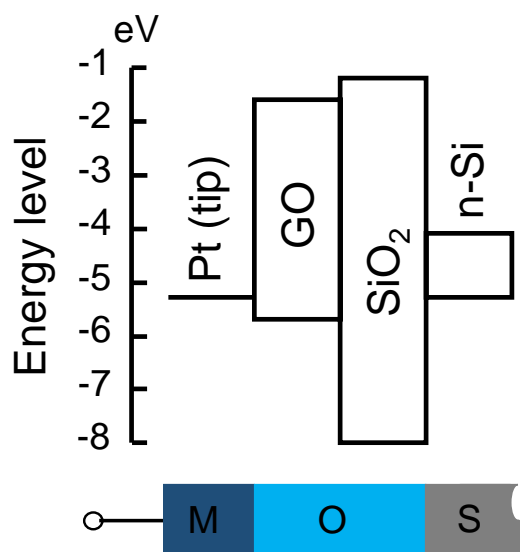


Fig. S9. The energy levels of the elements composing the metal–oxide–semiconductor (MOS) structure.

## 10. SEM images of AFM tip

Fig. S10 shows scanning electron microscopy (SEM, Magellan400) images of the Pt-coated tip before and after the AFM measurements. The tip size and shape before and after the AFM measurements did not change, within the error of measurement; the curvature radius remained at  $50 \text{ nm} \pm 10$ .

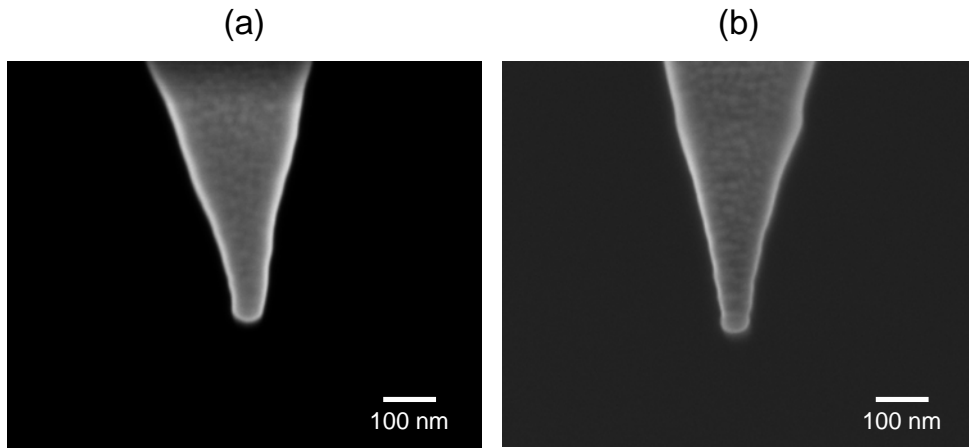


Fig. S10. SEM images of the Pt-coated tip (a) before and (b) after AFM measurements on the GO sheet.

## 11. Scanning transmission X-ray microscopy (STXM)

Fig. S11 shows STXM images and C K-edge spectra of the GO sheet on lacey carbon at a photon energy of 304.6 eV. The A and B regions show the free-standing GO sheet, and the C region shows the GO sheet on lacey carbon. The  $\pi^*/\sigma^*$  ratio in the A region is higher (0.66) than in the B (0.41) and C (0.59) regions. The peak of  $I_3$  (288.5 eV) in the C region, which originated from the  $\pi^*(C=O)$  states of COOH, is relatively low. Therefore, the lacey carbon shows a distinct ratio of  $\pi^*/\sigma^*$ , compared with the A and B regions.

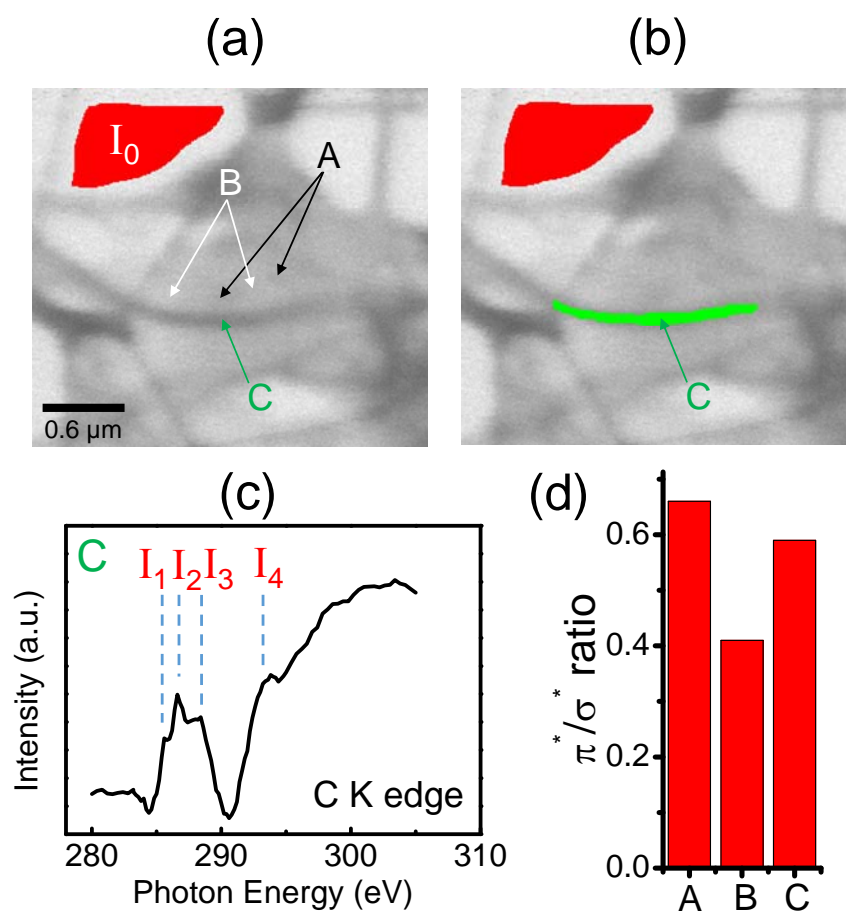


Fig. S11. STXM images (a) before and (b) after marking the C region. The  $I_0$  region is marked by red in an empty area for reference. (c) C K-edge spectra of the C region in (b).  $I_1$  and  $I_4$  are the unoccupied  $\pi^*$  and  $\sigma^*$  states, respectively, and  $I_2$  and  $I_3$  originate from  $\pi^*(\text{C-O-C})$  with the  $\pi^*(\text{C-OH})$  and  $\pi^*(\text{C=O})$  states of COOH, respectively. (d) Bar graph of the  $\pi^*/\sigma^*$  ratio at different positions. A, B, and C are the bright and dark regions in the free-standing GO sheet, and the lacey-carbon-supported GO sheet, respectively.

## References

1. J. I. Paredes, S. Villar-Rodil, A. Martínez-Alonso and J. M. D. Tascón, *Langmuir*, 2008, **24**, 10560-10564.
2. K. J. Kim, H. Lee, J. H. Choi, Y. S. Youn, J. Choi, H. Lee, T. H. Kang, M. C. Jung, H. J. Shin, H. J. Lee, S. Kim and B. Kim, *Adv. Mater.*, 2008, **20**, 3589-3591.
3. P. Wang, Y. Zhai, D. Wang and S. Dong, *Nanoscale*, 2011, **3**, 1640-1645.
4. O. C. Compton, B. Jain, D. A. Dikin, A. Abouimrane, K. Amine and S. T. Nguyen, *ACS Nano*, 2011, **5**, 4380-4391.
5. J. Chen, S. Liu, W. Feng, G. Zhang and F. Yang, *Phys. Chem. Chem. Phys.*, 2013, **15**, 5664-5669.
6. L.-F. Wang, T.-B. Ma, Y.-Z. Hu and H. Wang, *Phys. Rev. B*, 2012, **86**, 125436.
7. J. T. Robinson, F. K. Perkins, E. S. Snow, Z. Wei and P. E. Sheehan, *Nano Lett.*, 2008, **8**, 3137-3140.